

Molecular Cancer Therapeutics



A Novel Small Molecule Aurora Kinase Inhibitor Attenuates Breast Tumor Initiating Cells and Overcomes Drug Resistance

Fei-Meng Zheng, Zi-Jie Long, Zhi-Jie Hou, et al.

Mol Cancer Ther Published OnlineFirst June 4, 2014.

Updated version	Access the most recent version of this article at: doi: 10.1158/1535-7163.MCT-13-1029
Supplementary Material	Access the most recent supplemental material at: http://mct.aacrjournals.org/content/suppl/2014/06/04/1535-7163.MCT-13-1029.DC1.html
Author Manuscript	Author manuscripts have been peer reviewed and accepted for publication but have not yet been edited.

E-mail alerts	Sign up to receive free email-alerts related to this article or journal.
Reprints and Subscriptions	To order reprints of this article or to subscribe to the journal, contact the AACR Publications Department at pubs@aacr.org .
Permissions	To request permission to re-use all or part of this article, contact the AACR Publications Department at permissions@aacr.org .

A Novel Small Molecule Aurora Kinase Inhibitor Attenuates Breast Tumor Initiating Cells and Overcomes Drug Resistance

Fei-Meng Zheng^{1,2*}, Zi-Jie Long^{3*}, Zhi-Jie Hou^{2*}, Yu Luo⁴, Ling-Zhi Xu², Jiang-Long Xia², Xiao-Ju Lai¹, Ji-Wei Liu², Xi Wang¹, Muhammad Kamran², Min Yan¹, Shu-Juan Shao⁵, Eric W.-F. Lam⁶, Shao-Wu Wang², Gui Lu^{4§}, Quentin Liu^{1, 2, 3§}

¹ Sun Yat-sen University Cancer Center; State Key Laboratory of Oncology in South China; Collaborative Innovation Center of Cancer Medicine, Guangzhou 510060, China

² Institute of Cancer Stem Cell, Institute of Cancer Stem Cell - First Affiliated Hospital Collaborative Innovation Center of Oncology, Dalian Medical University, Dalian 116044, China

³ Department of Hematology, Third Affiliated Hospital, Sun Yat-sen University, Guangzhou 510630, China

⁴ Institute of Medicinal Chemistry, School of Pharmaceutical Sciences, Sun Yat-sen University, 132 Waihuan Road East, Guangzhou 510006, China

⁵ Department of Histology and Embryology, Dalian Medical University, Dalian 116044, China

⁶ Department of Surgery and Cancer, Imperial Centre for Translational and Experimental Medicine (ICTEM), Imperial College London, London, UK

* These authors contributed equally to this work.

[§] Correspondence to:

Quentin Liu, State Key Laboratory of Oncology in South China, Cancer Center, Sun Yat-sen University & Institute of Cancer Stem Cell, Dalian Medical University;
E-mail: liuq9@mail.sysu.edu.cn

Gui Lu, Institute of Medicinal Chemistry, School of Pharmaceutical Sciences, Sun Yat-sen University; E-mail: lugui@mail.sysu.edu.cn

Running title: AKI603 attenuates breast cancer initiating cells

Keywords: Aurora kinase, Small molecule inhibitor, Tumor-initiating cells, Breast cancer, Drug resistance

Abbreviations:

Aurora kinase A, AurA; Tumor-initiating cells, TICs; Embryonic stem cells, ESCs; Side population, SP; Combined index, CI; Three-dimensional (3D) culture model, 3D culture model.

Conflict of interest: The authors declare no conflict of interest.

Financial support:

This work was supported by the National Basic Research Program of China (973 Program; No. 2012CB967000 to Q. Liu), the National Natural Science Foundation

of China (No. 81130040 to Q. Liu, No.81000217 to Z.-J. Long and No.81201547 to M. Yan), Innovative Research Team in University of Ministry of Education of China (No. IRT13049 to Q. Liu) and the Science and Technology Foundation of Guangzhou (No. 2012J2200077 to Z.-J. Long).

Abstract

Chemoresistance is a major cause of cancer treatment failure. Tumor-initiating cells (TICs) have attracted a considerable amount of attention due to their role in chemoresistance and tumor recurrence. Here, we evaluated the small molecule Aurora kinase inhibitor AKI603 as a novel agent against TICs in breast cancer. AKI603 significantly inhibited Aurora-A (AurA) kinase and induced cell cycle arrest. In addition, the intra-gastric administration of AKI603 reduced xenograft tumor growth. Interestingly, we found that breast cancer cells that were resistant to epirubicin expressed a high level of activated AurA and also have a high CD24^{Low}/CD44^{High} TIC population. The inhibition of AurA kinase by AKI603 abolished the epirubicin-induced enrichment of TICs. Moreover, AKI603 suppressed the capacity of cells to form mammosphere and also suppressed the expression of self-renewal genes (β -catenin, c-Myc, Sox2 and Oct4). Thus, our work suggests the potential clinical use of the small molecule Aurora kinase inhibitor AKI603 to overcome drug resistance induced by conventional chemotherapeutics in breast cancer.

Introduction

Breast cancer is one of the most common malignancies and is a leading cause of mortality in women (1). Although treatment strategies that combine surgery with adjuvant chemotherapy improve survival rates, a significant portion of patients eventually acquire resistance to chemotherapeutic agents. Chemoresistance can be a consequence of cell intrinsic genetic changes, such as reprogramming of metabolic pathways, up-regulation of drug efflux pumps, activation of detoxifying enzymes or apoptotic defects (2, 3). Additionally, chemoresistance can also result from cell extrinsic factors, such as cytokines and growth factors (4, 5). The intrinsic or extrinsic mechanisms of chemoresistance have been demonstrated to be a major cause of cancer treatment failure. Thus, strategies to overcome chemoresistance are urgently needed.

The cancer stem cell (CSC) hypothesis offers new insight into the mechanism of chemoresistance. The CSC hypothesis states that a small population of cancer cells, also termed tumor-initiating cells (TICs), has undifferentiated phenotypes, an increased capacity for self-renewal and the ability to form new tumors (6-8). The characteristics that differentiate TICs from other tumor cells are high expression of levels of drug efflux transporter proteins and detoxification enzymes (9, 10). These molecules are responsible for protecting TICs from drug damage and for producing chemoresistant clones. Therefore, eradicating TICs could be a therapeutic avenue for overcoming chemoresistance.

Aurora-A (AurA) belongs to the Aurora family of serine/threonine kinases, which

are central for mitotic progression (11). Small molecule kinase inhibitors of AurA have attracted considerable interest due to its overexpression in various tumor types, and because of its function as an oncogene depending on the kinase activity (12, 13). Recent studies suggest that the kinase activity of AurA is responsible for chemoresistance as it overrides cell cycle checkpoint (14-17). AurA also plays an important role in the tumorigenicity and chemoresistance of colorectal TICs (18). However, whether the kinase activity of AurA could be a potential anti-TIC target for overcoming chemoresistance remains unclear.

In the present study, we explored the potential anti-TIC role of the novel small molecule Aurora kinase inhibitor AKI603. We demonstrated that AKI603 inhibited AurA kinase and xenograft tumor growth. Interestingly, epirubicin-resistant cells displayed enhanced AurA kinase activity and were enriched in CD24^{Low}/CD44^{High} TICs population. Targeting AurA kinase activity with AKI603 potently suppressed the epirubicin-induced accumulation of CD24^{Low}/CD44^{High} TICs. Thus, we presented a novel mechanism by which the inhibition of AurA kinase can overcome chemoresistance by abolishing the accumulation of TICs. This mechanism has important implications for cancer therapy.

Materials and Methods

Synthesis of AKI603

AKI603 was designed and synthesized by our lab. The synthetic route was shown in Supplementary Figure S1A. 2,4,6-trichloropyrimidine was treated <1> with 3-amino-5-methylpyrazole <2>, which afforded the C4-substituted pyrimidine <3> regioselectively. Next intermediate 5 was generated via nucleophilic substitution at the C2-position of the pyrimidine core in the presence of 4-nitroaniline <4>. Microwave-assisted substitution at the C6-position of the pyrimidine ring with 1-methylpiperazine <6> yielded AKI603.

Reagents and cell culture

AKI603 was dissolved in dimethyl sulfoxide (DMSO) to a stock concentration of 100mM and was stored at -20°C. Epirubicin was dissolved in H₂O to a stock concentration of 100mM and was stored at -20°C. The human breast cancer cell lines BT549, MCF-7, Sk-br-3, MDA-MB-231, MDA-MB-453 and MDA-MB-468 were obtained from the American Type Culture Collection (ATCC). The cell lines were authenticated at ATCC before purchase by their standard short tandem repeat DNA typing methodology. Epirubicin resistant MCF-7 (MCF-7-Epi) cells were previously described (19), and were authenticated by the standard short tandem repeat DNA typing methodology. SUM149 cells were kindly provided by Prof. Zhi-Min Shao (Department of Medical Oncology, Cancer Hospital of Fudan University, Shanghai Medical College, China), and were authenticated by the standard short tandem repeat DNA typing methodology. Each cell line was cultured in its standard medium as

recommended by ATCC. MCF-7-Epi cells were cultured in DMEM (Gibco) supplemented with 10% fetal bovine serum (FBS; Hyclone). SUM149 cells were cultured in F-12 Hams (Gibco) supplemented with 5% fetal bovine serum (FBS; Hyclone), 5µg/ml insulin (Sigma) and 1µg/ml hydrocortisone (Sigma). All cell lines used in this study were obtained in 2013, and were used within 6 months of receipt for this study.

Kinase activity assay

The kinase activity of AurA was measured using the Caliper Mobility Shift Assay. Briefly, 3-fold dilutions of a 10 µM stock of AKI603 (a total of 10 concentrations) were tested. AKI603, AurA, the FAM-labeled peptide and ATP were added in a 384-well format, and the plate was incubated at 28°C for 1 h. The reaction was stopped by the addition of a stop buffer and the data were collected with a LabChip EZ reader (PerkinElmer).

Cell cycle analysis

The cells were treated with the indicated concentrations of AKI603 for 48 h, collected and fixed in ice-cold alcohol (75%). After an overnight incubation at 4°C, the cells were collected by centrifugation, and were resuspended in a PI (Sigma) staining solution (PI: 50µg/ml, RNase A: 100µg/ml, Triton X-100: 0.2% in PBS, 1ml/sample) at a concentration of 1.0×10^6 cells/ml. After PI staining, the quantification of the cell cycle distribution was carried out using a flow cytometer (Beckman) equipped with the Multicycle software (Phoenix).

CD24 and CD44 expression analysis

To evaluate CD24 and CD44 expression, 2×10^5 cells were plated in dishes ($\Phi=6\text{cm}$) and were cultured with the indicated concentrations of AKI603 and/or epirubicin for the indicated times. The cells were harvested and incubated with anti-human CD24 PE (eBioscience) and anti-human CD44 FITC (eBioscience) at 4°C for 0.5 h in the dark. The cells were then resuspended in 1ml of PBS and subjected to flow cytometric analysis.

Fluorescence-activated cell sorting (FACS)

To purify the $\text{CD24}^{\text{Low}}/\text{CD44}^{\text{High}}$ and $\text{CD24}^{\text{High}}/\text{CD44}^{\text{High}}$ populations, 1×10^7 exponentially growing cells were harvested and incubated with anti-human CD24 PerCP-eFluor® 710 (eBioscience) and anti-Human CD44 FITC (eBioscience) at 4°C for 0.5 h in the dark. Next, the cells were resuspended in 3ml of PBS and subjected to sorting.

Immunofluorescence staining

The cells incubated with $0.6\mu\text{M}$ AKI603 for 24 h were fixed in paraformaldehyde for 15 min at 4°C and were permeabilized in 0.5% TritonX-100 in PBS at room temperature (RT) for 10 min. The cells were then incubated with 1% BSA for 1 h at RT to block nonspecific binding prior to the addition of the primary antibody. The slides were incubated with the primary antibodies to Aur-A (Upstate), α -Tubulin (Sigma) at RT for 1 h followed by an Alexa Fluor 488- or 546-conjugated secondary antibody (Invitrogen). After counterstaining with DAPI ($1\mu\text{g}/\text{ml}$, Sigma), the cells were visualized using a confocal microscope ($630\times$, Olympus).

Western blot analysis

The cells treated with indicated concentration of AKI603 for 48 h were harvested and were lysed in RIPA buffer. The protein concentrations were determined by the Bradford method using BSA (Sigma) as the standard. Equal amounts of cell extract were subjected to electrophoresis in SDS-polyacrylamide gel and were transferred to nitrocellulose membrane (Millipore). The membranes were blocked and then incubated with GAPDH (Ambion), β -Actin (Santa Cruz), pAurA (Thr288, Cell Signaling Technology), pAurA/B (Cell Signaling Technology), AurA (Upstate), AurB (Cell Signaling Technology), HA-tag (Sigma), β -catenin (Cell Signaling Technology), c-Myc (Santa Cruz), Sox2 (Epitomics), Oct4 (Epitomics) and Nanog (Epitomics) primary antibodies at 4°C overnight. Next, the membranes were incubated for 1 h at RT with the appropriate secondary antibodies. Antibody binding was detected with an enhanced chemiluminescence kit (Pierce).

Mammosphere formation assay

The mammosphere formation assay was performed as previously described (20). A single cell suspension was obtained by trypsinization. Clumped cells were excluded with a 40 μ m sieve, and the suspension was analyzed microscopically for single-cellularity. The percentage of clumped cells was <5%. Single cells were plated in ultralow attachment 6-well plates at a low density of 1000 viable cells/ml. The cells were maintained in DMEM/F12 (Gibco) supplemented with B27 (Invitrogen), 20 ng/ml EGF (Sigma), 20 ng/ml bFGF (BD Biosciences) and 4 μ g/ml heparin (Sigma) for 10 days. The mammospheres were photographed using inverted microscope (100 \times , Olympus). The diameters of the mammospheres were calculated with the Image pro

plus 6.0 software (Media Cybernetics).

Plate colony formation assay

The cells were plated at 1×10^3 cells/well and were treated with the indicated concentrations of AKI603 and/or epirubicin for 6 days. The cells were then fixed in 2% PFA and stained with a 0.05% crystal violet solution (Sigma). The number of colonies was counted.

Annexin V/PI analysis

Adherent cells were treated with the indicated concentrations of AKI603 or epirubicin, collected and resuspended in the binding buffer. Annexin-V-FITC and PI was added to the cells according to the protocol contained in the Annexin V-FITC Apoptosis Detection Kit (EMD Biosciences). The samples were then incubated for 15 min in the dark at 4°C and subjected to flow cytometric analysis.

Combination index (CI) calculation

The data acquired from the MTT assay were used to evaluate the combination index. The combination index was analyzed with the CompuSyn software using the average fraction of cells that responded to each drug (21). CI values of less than 0.8, between 0.8 and 1.2 and more than 1.2 were defined as synergistic, additive and antagonistic, respectively (22).

Three-dimensional culture

Eight-chambered RS glass slides (BD Falcon) were pre-coated with 40µl/well of Matrigel (BD Biosciences). The Matrigel was solidified at 37 °C for 30 min. Next, the cells were suspended in growth medium containing a final concentration of 2%

Matrigel and plated at a density of 2500 cells/well. The cells were fed with growth medium containing 2% Matrigel every 4 days. After 10 day of culture, the cells were photographed using an inverted microscope. The diameters were calculated with Image pro plus 6.0 software.

Primary breast cancer cell isolation

After obtaining informed consent, breast cancer specimens were collected from patients undergoing surgery in accordance with the Institutional Review Boards of the Sun Yat-sen University Cancer Center. Breast lesions were classified by histologic diagnostic assessment and were sampled by pathologists. The lesions were mechanically and enzymatically dissociated to yield clumps of epithelial cells, termed organoids, by incubation at 37°C for 2 hours in a 1:1 solution of collagenase I (3mg/mL):hyaluronidase (100U/mL) (Sigma). After filtration through a 40 µm pore filter and washing with PBS, the organoids from the tumor tissue were trypsin dissociated to single cells for subsequent experiments.

Tumor growth in xenografts

MCF-7-Epi cells (7.5×10^6) were injected into the right flank of 4-week-old female nude mice (n=5). The mice were not supplemented with estrogen, as previous studies showed that drug-resistant MCF-7 cells do not require estrogen signaling to form tumors in nude mice (23, 24). On day 30, the mice (tumor size $\sim 50\text{mm}^3$) were randomly distributed into two groups that were treated intra-gastrically every day with either a vehicle control or with 50 mg/kg AKI603 dissolved in PEG300. The tumor volumes ($A \times B^2/2$; A being the greatest diameter and B being the diameter

perpendicular to A) were measured by calipers. Other indicators of general health such as body weight, feeding behavior and motor activity of each animal were also monitored. After the administering the drug or vehicle for 14 days, the mice were fed for a another 14 days. At day 59, the mice were sacrificed and the tumor xenografts were immediately dissected, weighed, stored and fixed. All animal procedures were approved by the Institutional Animal Care and Use Committee of the Sun Yat-sen University Cancer Center.

Statistics

Statistical analyses were performed using the SPSS software, version 16.0 (SPSS Inc.) or with GraphPad Prism 5.0 (GraphPad Software, Inc.). The Kruskal-Wallis test, followed by Dunn's Multiple Comparison test, was used to perform a statistical comparison with regard to mammospheres size distribution. The unpaired Student's t test was used to perform a statistical comparison between two groups. The ANOVA test, followed by Least Significant Difference test, was used when performing multiple comparison. The level of significance was set at $p < 0.05$.

Results

AKI603 inhibits AurA activity, induces cell cycle arrest and suppresses proliferation in breast cancer cells.

The chemical structure of AKI603 was shown in Figure 1A. To assess whether AKI603 inhibited AurA kinase activity, an *in vitro* kinase activity assay was performed. As shown in Figure 1B, the IC₅₀ of AKI603 was determined to be 12.3±1.5nM. To evaluate the effect of AKI603 on breast cancer cell proliferation, eight breast cancer cell lines were treated with AKI603 for 48 h, and the rate of cell proliferation was determined by an MTT assay. The clinicopathological features of the eight cell lines have been previously summarized (25). As shown in Supplementary Figure S1B, all of the tested breast cancer cell lines were sensitive to AKI603 and showed typical sigmoidal log (dose)-response curves. A cell counting assay was also performed to confirm the MTT results for the MDA-MB-453 and MDA-MB-468 cells (Supplementary Fig. S1C). The *in vitro* IC₅₀s, as measured by sigmoidal curve fitting for each cell line, were summarized in Supplementary Figure S1D. The IC₅₀s that were acquired by the MTT assay were consistent with the cell counting experiments. Next, we examined whether AKI603 inhibited the kinase activity of AurA in breast cancer cells, by examining the phosphorylation of AurA Thr288. As shown in Figure 1C, treatment with 0.6 μM or higher concentrations of AKI603 for 48 h significantly inhibited Thr288 phosphorylation (detected with pAurA) in all cell lines tested. The total AurA protein levels were marginally reduced or not changed. Moreover, we evaluated the inhibitory activity of AKI603 against AurB by detecting Thr232

phosphorylation in SUM149 and BT549 cells. We found that AKI603 also inhibited AurB kinase activity (Fig. 1C). The inhibitory activity of AKI603 toward AurB kinase was lower than that toward AurA kinase as determined by western blotting (Fig. 1C).

Due to the crucial role of AurA in mitosis, we determined whether inhibition of AurA kinase activity by AKI603 could block the cell cycle in SUM149, BT549, MCF-7, MCF-7-Epi, Sk-br-3 and MDA-MB-231 cells. After treatment with 0.6 μ M AKI603, SUM149 cells were fixed and stained with the indicated antibodies, and the cells in mitosis was analyzed. As shown in Figure 1D, mitotic cells in the control group displayed mainly bipolar spindle (Fig. 1D, white arrow in the left panel). AurA (Fig. 1D, white arrow in left panel, green) localized at the region of the centrosomes and mitotic spindle. AKI603 treatment (Fig. 1D, white arrow in right panel) increased monopolar spindle formation compared with the control group (Fig. 1E, 7.40 \pm 0.02% VS 3.47 \pm 0.01%, $p=0.025$). A similar phenomenon was observed in BT549, MCF-7, MCF-7-Epi, Sk-br-3 and MDA-MB-231 cells (Supplementary Fig. S2). For cell cycle profile analysis, SUM149 cells were treated with 0.3 μ M or 0.6 μ M AKI603 for 48 h, and the DNA content was analyzed after PI staining. As shown in Figure 1F, with increasing concentrations of AKI603 from 0 μ M to 0.3 μ M and 0.6 μ M, the percentage of cells in G2/M phase (4N) was increased from 20.9 \pm 0.6% to 36.6 \pm 6.2% and 45.2 \pm 1.5%, respectively; Furthermore, the percentage of cells that contained more than 4N DNA was increased from 0.2 \pm 0.2% to 14.0 \pm 1.9% and 20.5 \pm 3.6%, respectively. Similar results were obtained with BT549, MCF-7, MCF-7-Epi, Sk-br-3 and MDA-MB-231 cells (Supplementary Fig. S3). These results suggested that the

inhibition of cell proliferation that was induced upon AKI603 treatment is associated with cell cycle blockage.

AurA kinase activity and CD24^{Low}/CD44^{High} TICs are elevated in epirubicin-resistant MCF-7 cells.

MCF-7-Epi cells were used to investigate the potential role of AurA kinase activity in the regulation of TICs and drug resistance. An MTT assay showed that MCF-7-Epi cells (IC₅₀=7.45±2.01μM) exhibited significant resistance toward epirubicin compared with wild-type MCF-7 cells (IC₅₀=0.38±0.09μM) (Fig. 2A). To confirm these results, a cell counting assay was performed. The results were consistent with those from the MTT assay (Fig. 2B). The kinase activity of AurA was significantly increased in MCF-7-Epi cells compared with wild type MCF-7 cells, suggesting that AurA kinase activity might be important for maintaining resistance to epirubicin. Self-renewal genes, including β-catenin, c-Myc, Sox2, Oct4 and Nanog, play key roles in maintaining stemness (26-33) and mediating chemoresistance (34-36). As shown in Figure 2C, the expression of β-catenin, c-Myc, Sox2, Oct4 and Nanog was also increased in MCF-7-Epi cells compared with wild type MCF-7 cells. Interestingly, flow cytometric analysis showed that MCF-7-Epi cells contained a higher percentage of CD24^{Low}/CD44^{High} TICs (26.6±3.5679%) than their wild-type counterparts (0.67±0.21%, *p*=0.0002, Fig. 2D). Indeed, our data indicated that the CD24^{Low}/CD44^{High} TIC population was more resistant to conventional chemotherapeutic agents than the CD24^{High}/CD44^{High} population (Supplementary Fig. S4). These results suggested that targeting the kinase activity of AurA might be a

potential strategy to deplete the CD24^{Low}/CD44^{High} TIC population in breast cancer.

The cytotoxic effects of genotoxic agents, such as epirubicin, might also be enhanced.

Inhibition of AurA by AKI603 suppresses stem cell properties in breast cancer cells.

We next asked if AKI603 targeted the CD24^{Low}/CD44^{High} TIC population in breast cancer cells. To evaluate whether AKI603 induced apoptosis, MCF-7-Epi cells were collected for flow cytometry analysis of AnnexinV/PI staining. Our results showed that MCF-7-Epi cells treated with 0.6 μ M of AKI603 did not undergo obvious apoptosis (Supplementary Fig. S5A). To determine if AKI603 has an anti-TIC effect, we first examined the short-term effects of AKI603 in the CD24^{Low}/CD44^{High} TIC population. Results showed that a short-term (<6 days) treatment of MCF-7-Epi cells with AKI603 did not show an obvious anti-TIC effect (Supplementary Fig. S5B). We further tested the long-term effect of AKI603 in the CD24^{Low}/CD44^{High} TIC population. MCF-7-Epi cells were treated with 0.6 μ M AKI603 or DMSO for 6 and 9 days, and the adherent cells were collected for flow cytometric analysis of CD24/CD44 expression. As shown in Figure 3A, before treatment (at day 1), both the DMSO control group (Fig. 3B, CD24^{Low}/CD44^{High} TIC population=25.1 \pm 1.6%) and the AKI603 treatment group (Fig. 3B, CD24^{Low}/CD44^{High} TIC population=23.8 \pm 4.0%) contained comparable proportions of CD24^{Low}/CD44^{High} cells ($p=0.6483$). The CD24^{Low}/CD44^{High} TIC population was gradually depleted by treatment with AKI603 (Fig. 3A, lower panel) at day 7 (Fig. 3B, CD24^{Low}/CD44^{High} TIC population=12.3 \pm 2.0%, $p=0.0081$) and day 10 (Fig. 3B, CD24^{Low}/CD44^{High} TIC

population=2.4±2.3%, $p=0.0006$), while the CD24^{Low}/CD44^{High} TIC population did not significantly change in the DMSO control group (Fig. 3A, upper panel and Fig. 3B, Day7: CD24^{Low}/CD44^{High} TIC population=25.4±4.2%; Day10: CD24^{Low}/CD44^{High} TIC population=25.4±3.3%). Similar results were obtained with SUM149 (Supplementary Fig. S5C) and BT549 cells (Supplementary Fig. S5D). We further evaluated whether the CD24^{Low}/CD44^{High} TICs from primary patient samples were sensitive to AKI603. We found that AKI603 also effectively depleted the CD24^{Low}/CD44^{High} TIC population of primary breast cancer cells (Supplementary Fig. S5E). Interestingly, the CD24^{Low}/CD44^{High} population of normal primary breast cells was insensitive to AKI603 (Supplementary Fig. S5E), indicating that AKI603 may exhibit low toxicity. To confirm that the disruption of AurA kinase activity resulted in anti-TIC effects in breast cancer cells, kinase dead mutants of AurA (K162M or D274N) (37, 38) were expressed in SUM149 cells (Fig. 3C). Indeed, the over-expression of either K162M or D274N reduced the CD24^{Low}/CD44^{High} TIC population in SUM149 cells (Fig. 3D). These effects were similar to the anti-TIC effects induced by AKI603.

Additionally, we examined the effects of AKI603 on mammosphere formation in breast cancer cells. To this end, MCF-7-Epi cells were maintained in mammosphere culture medium containing DMSO, 0.6µM or 1.2µM AKI603, and the mammosphere diameters and numbers were measured. As shown in Figure 3E and 3F, compared with controls, the mammosphere sizes were smaller when cultured with 0.6µM (Fig. 3E and 3F, $p<0.001$) and 1.2µM AKI603 (Fig. 3E and 3F, $p<0.001$). The number of

large mammospheres ($\Phi > 60 \mu\text{m}$) in the $0.6 \mu\text{M}$ (65 ± 18 mammospheres per 1000 cells, $p = 0.0001$) and $1.2 \mu\text{M}$ (27 ± 8 mammospheres per 1000 cells, $p = 0.0005$) AKI603 treatment groups was lower than in the DMSO control group (268 ± 29 large mammospheres per 1000 cells) (Fig. 3G). Similar results were also observed in SUM149 (Supplementary Fig. S5F-H) and BT549 cells (Supplementary Fig. S5I-K).

Next, we investigated the expression of several self-renewal genes in breast cancer cells after AKI603 treatment. Results showed that $0.6 \mu\text{M}$ concentration of AKI603 significantly inhibited AurA activity in all tested breast cancer cell lines (Fig. 1C). Meanwhile, AKI603 suppressed the expression levels of the self-renewal genes, including β -catenin, c-Myc, Sox2, Oct4 and Nanog in a dose-dependent manner (Fig. 3H and Supplementary Fig. S6A).

AKI603 abolishes epirubicin enriched CD24^{Low}/CD44^{High} TICs, and suppresses self-renewal genes expression and mammosphere formation.

We next explored the combinational effects of epirubicin and AKI603 in breast cancer cells. The long-term (6 days) growth inhibitory effects of low doses of AKI603 were determined with an MTT assay. The dose that inhibited cell proliferation by 20% was chosen for further investigations on the anti-TICs effects. As shown in Supplementary Figure S6B, in SUM149 cells, $0.078 \mu\text{M}$ of AKI603 or $0.078 \mu\text{M}$ epirubicin alone inhibited cell proliferation by approximately 20% after 6 days of treatment in SUM149 cells. Flow cytometric analysis showed that incubation with a control solvent did not significantly change the ratio of CD24^{Low}/CD44^{High} TIC population at Days 1, 7 and 10 ($35.2 \pm 2.24\%$, $34.7 \pm 2.70\%$ and $33.3 \pm 2.16\%$,

respectively; Fig. 4A and 4B). Interestingly, epirubicin alone resulted in an enrichment of CD24^{Low}/CD44^{High} TIC population, with the percentages at Day 1, 7 and 10 were 34.3±2.70%, 43.1±2.46% and 60.6±10.10%, respectively (Fig. 4A and 4B). For AKI603 treatment, the CD24^{Low}/CD44^{High} TIC population at Day 1, 7 and 10 were 34.16±2.10%, 10.0±2.03% and 6.0±1.72%, respectively (Fig. 4A and 4B). Crucially, when SUM149 were treated with epirubicin and AKI603 together, the epirubicin-induced enrichment of the CD24^{Low}/CD44^{High} TIC population was abolished. Under these conditions, the CD24^{Low}/CD44^{High} TIC population at Day 1, 7 and 10 were 34.2±2.86%, 11.8±2.61% and 4.1±1.02%, respectively (Fig. 4A and 4B). Similar findings were observed in MCF-7 cells (Supplementary Fig. S6C and S6D).

In SUM149 cells, the expression of AurA, pAurA and self-renewal genes was also analyzed by western blot analysis. As shown in Figure 4C, the expression levels of tested markers were relatively stable in the control groups (Fig. 4C, compare lanes 2-3 with lane 1). However, in the epirubicin-treated cells (Fig. 4C, compare lanes 5-6 with lane 4), pAurA and Nanog were significantly increased, c-Myc and Oct4 were decreased, AurA, β -catenin and Sox2 expression levels did not change significantly. The elevated expression of pAurA and Nanog suggested that these proteins might be responsible for the epirubicin resistance and the enriched CD24^{Low}/CD44^{High} TIC population. In the AKI603 treated cells (Fig. 4C, compare lanes 8-9 with lane 7), the expression levels of pAurA as well as that of β -catenin, c-Myc, Sox2, Nanog and Oct4 were significantly suppressed. Importantly, for the cells exposed to the epirubicin/AKI603 combination, AKI603 reversed the epirubicin-induced

up-regulation of pAurA and Nanog. Furthermore, the combination of epirubicin and AKI603 resulted in a greater inhibition of β -catenin, c-Myc, Sox2 and Oct4 expression (Fig. 4C, compare lanes 10-12 with lane 4-6).

Moreover, we evaluated the combinational effects of AKI603 and epirubicin on mammosphere formation using SUM149 cells. As shown in Figure 4D and 4E, epirubicin alone ($p<0.001$) or AKI603 alone ($p<0.001$) slightly reduced mammosphere size compared with the control group. When the SUM149 cells were treated with epirubicin and AKI603 simultaneously, mammosphere formation was significantly blocked ($p<0.001$, Fig. 4D and 4E). As shown in Figure 4F, AKI603 decreased the formation of large mammospheres (125 ± 35 mammospheres per 1000 cells, $p=0.0319$) compared with the control group (187 ± 30 mammosphere per 1000 cells), whereas epirubicin did not significantly down-regulate the formation of large mammosphere (182 ± 21 mammospheres per 1000 cells, $p=0.4336$). However, the combination of epirubicin and AKI603 potently inhibited the formation of large mammospheres (11 ± 2 mammospheres per 1000 cells, $p=0.0106$).

AKI603 synergistically enhances the cytotoxic effects of epirubicin in breast cancer cells.

Chemotherapy with high-doses of chemotherapeutic reagents often causes side effects. Therefore, new strategies to allow for treatment with lower dose chemotherapy are urgently needed. Synergistic analysis was performed to evaluate the interactions between AKI603 and epirubicin in breast cancer cell lines. The experimental setting of AKI603 and epirubicin treatment was the same as in

Supplementary Figure S6B, where AKI603 and epirubicin were combined in a fixed ratio (1:1). The results showed that the combination therapy resulted in a greater growth inhibition of SUM149 cells (Fig. 5A, labeled in green, $IC_{50}=0.089\pm 0.02\mu M$) than was achieved with either AKI603 (Fig. 5A, labeled in red, $IC_{50}=0.41\pm 0.09\mu M$) or epirubicin alone (Fig. 5A, labeled in blue, $IC_{50}=0.41\pm 0.15\mu M$). This result, which was achieved using an MTT assay, was confirmed by cell counting (Fig. 5B). The average fraction of cells that responded to each drug was subjected to combination index (CI) analysis (21). As shown in Figure 5C and 5D, AKI603 and epirubicin acted synergistically to inhibit SUM149 cell proliferation. Similar findings were observed for BT549 (Supplementary Fig. S6E and S6F) and MCF-7 cells (Supplementary Fig. S6G and S6H). To confirm these results, a drug concentration of $0.078\mu M$ was used in a colony formation assay. As shown in Figure 5E and 5F, in SUM149 cells, AKI603 ($78.8\pm 9.2\%$, $p=0.0161$) and epirubicin ($73.8\pm 5.7\%$, $p=0.0013$) alone marginally inhibited colony formation compared with the control groups, while the combination ($10.3\pm 3.3\%$, $p<0.001$) substantially suppressed colony formation compared with control group. Furthermore, a three-dimensional (3D) culture model was used to mimic the *in vivo* tissue environment. Compared to *in vivo* animal models, the 3D culture model is a more purified system with high reproducibility, and experimental results can be recorded in real-time (39). Thus, 3D culture model was used to confirm the enhanced efficacy of the epirubicin/AKI603 drug combination. Indeed, AKI603 enhanced the cytotoxicity of epirubicin in this three-dimensional culture model (Fig. 5G and 5H). Our results suggested that the inhibition of AurA by

AKI603 provided a potential strategy by which the concentrations of genotoxic chemotherapeutic agents can be lowered in the treatment of cancer.

AKI603 attenuates xenograft tumor growth.

To evaluate the *in vivo* anti-cancer effects of AKI603, we employed a xenograft model. Nude mice bearing MCF-7-Epi xenograft tumors were treated with AKI603 (50 mg/kg, q.d.) by intra-gastric administration for 14 days. As shown in Figure 6A and 6B, the tumor size in the AKI603-treated group ($172 \pm 69 \text{ mm}^3$, $p=0.0136$) was smaller than that in control group ($367 \pm 119 \text{ mm}^3$), indicating that the growth of xenograft tumors was significantly inhibited by AKI603. Consistently, the tumor weight in the AKI603-treated group ($0.1121 \pm 0.0973 \text{ g}$, $p=0.0159$) was significantly lower than that in control group ($0.3829 \pm 0.1807 \text{ g}$, Fig. 6C). During the experimental period, the mice in the AKI603-treated group showed a slight decrease in body weight (Fig. 6D), indicating the low toxicity of intra-gastrically administered AKI603.

Discussion

In the present study, we evaluated the anti-TIC effects of a novel small molecule Aurora kinase inhibitor AKI603. We showed that AKI603 effectively inhibited AurA kinase activity and xenograft tumor growth (Fig. 1B, 1C and Fig. 6). Epirubicin kinase activity and xenograft tumor growth (Fig. 1B, 1C and Fig. 6). Epirubicin treatment induced the up-regulation of AurA kinase activity (Fig. 2C and 4C) and an enrichment in the CD24^{Low}/CD44^{High} TIC population (Fig. 4A, 4B and Supplementary Fig. S6C, S6D). Surprisingly, AKI603 abolished this epirubicin-induced CD24^{Low}/CD44^{High} TIC population enrichment (Fig. 4A, 4B and Supplementary Fig. S6C, S6D) and overcame epirubicin resistance (Fig. 4D-4F and Fig. 5).

The development of chemoresistance is a major hindrance to the effective treatment of cancer. The mechanism of chemoresistance is complicated due to numerous factors contributing to the regulation of drug sensitivity, such as accelerated drug efflux, drug inactivation, DNA damage repair and the evasion of apoptosis (40). Traditional chemotherapies target rapidly dividing cancer cells and effectively lower the tumor burden. However, a small fraction of cancer cells, termed TICs, remain quiescent in the G0 phase and express high levels of drug efflux transporter proteins and detoxification enzymes (9, 10). Our data suggested that chemoresistance might result from an enrichment in TICs in response to chemotherapeutics (Fig. 2 and Fig. 4A-4C). Over a period of chemotherapeutic treatment, TICs survive and can subsequently form a new tumor with a chemoresistant phenotype. Consistent with this notion, previous reports show that CD34⁺/CD38⁻ leukemic precursors exhibit increased resistance to daunorubicin in comparison with their CD34⁺/CD38⁺ counterparts. The

CD34⁺/CD38⁻ progenitors also express higher expression levels of multidrug resistance genes and have lower levels of Fas/Fas-L and Fas-induced apoptosis compared with CD34⁺/CD38⁺ blasts (41). Moreover, the treatment of KG1a leukemic cells with 50µg/ml of 5-FU for 4 days enriches the CD34⁺/CD38⁻ subpopulation more than 10 fold. These cells show higher levels of ABCG2 and an increase side population compared with untreated cells (42). Indeed, the CD24^{Low}/CD44^{High} TIC population displayed higher drug resistance compared with the CD24^{High}/CD44^{High} population in breast cancer (Supplementary Fig. S4). These results from our group and others suggested that TICs could be targeted in an effort to overcome chemoresistance.

AurA regulates multiple critical mitotic processes (11, 43), including cell fate determination. In *Drosophila* bearing AurA with a mutation in the catalytic domain, Numb is distributed uniformly around the cell cortex during mitosis and is separated equally into the two daughter cells. This uniform distribution of Numb lead to cell fate changes in the sensory organ precursor lineage (44). *Drosophila* bearing another mutation of AurA had an increases number of brain neuroblast numbers (45). Most recently, a study shows that AurA is necessary for embryonic stem cell maintenance. AurA phosphorylated Ser212 and Ser312 of p53 to control ectodermal and mesodermal differentiation (46). While a role for AurA kinase activity in the control of cell fate determination in normal stem cells has been well documented, it is not known if it is similarly involved in cancer. Our data showed that the inhibition of AurA activity by AKI603 reduced the CD24^{Low}/CD44^{High} TIC population and

decreased mammosphere formation and self-renewal gene expression (Fig. 3). Consistently, the over-expression of kinase dead AurA had similar inhibitory effect on the CD24^{Low}/CD44^{High} TIC population in SUM149 cells (Fig. 3D), suggesting that AurA kinase activity was important for maintaining the TICs population. Interestingly, our data showed that AKI603 also inhibited AurB kinase activity. However, the inhibitory effect of AKI603 on AurB was lower than that on AurA. These data indicated that AurB might also be involved in maintaining TICs population.

Consistent with our finding that the inhibition of AurA increased cell sensitivity to conventional chemotherapeutic drugs (Fig. 5), previous studies indicate that the kinase activity of AurA is critical for overriding cell cycle checkpoints in cancer, and that it is therefore responsible for the chemoresistance that occurs upon AurA overexpression (14-17). In addition, a recent report demonstrates that the Aurora kinase inhibitor CCT129202 increases the sensitivity of ABCB1/ABCG2-overexpressing cells and side population cells to chemotherapeutic drugs by inhibiting the function of drug efflux pumps (47). In the present study, we showed that AKI603 displayed novel anti-TIC effects with long-term treatment (≥ 6 days) (Fig. 3A and 4A). Short-term treatments with AKI603 did not have obvious anti-TIC effects (Supplementary Fig. S5B). Our study showed that the cells treated with AKI603 contained less TIC population and did not undergo obvious apoptosis (Supplementary Fig. S5A). These results suggested that AKI603 might cause a shift from a TIC population to a non-TIC population instead of inducing TIC death. Thus, short-term treatment (2 days) with AKI603 primarily had effects on non-TICs.

Importantly, we observed that a long-term treatment with AKI603 indeed inhibited the epirubicin-induced enrichment of TICs and had synergistic effects with epirubicin on proliferation (Fig. 4A and 5A). Thus, our data also provided a new drug combinational strategy to reduce the dose-related side effects of chemotherapeutics for clinical therapy.

One of the most important characteristics of stem cells is their capacity for self-renewal. Numerous factors, such as Wnt/ β -catenin, c-Myc, Sox2, Oct4 and Nanog, play key roles in regulating the balance between the self-renewal and differentiation of stem cells (26-29). For example, Sox2 overexpression increases mammosphere formation, while the suppression of Sox2 suppresses mammosphere formation and delays tumor progression in xenograft tumor initiation models (32). In addition, the overexpression of Oct4 promotes the dedifferentiation of melanoma cells to tumor-initiating-like cells, while the knockdown of Oct4 in dedifferentiated cells lead to a loss of TIC phenotypes (31). Moreover, Nanog regulates self-renewal of TICs through the insulin-like growth factor pathway in human hepatocellular carcinoma (33). In agreement with these studies, our data suggested that epirubicin significantly stimulated the kinase activity of AurA (Fig. 2C and Fig. 4C). We also found that the protein levels of self-renewal gene, β -catenin, c-Myc, Sox2, Oct4 and Nanog, were up-regulated in epirubicin resistant cells (Fig. 2C). AKI603 repressed AurA activity and decreased β -catenin, c-Myc, Sox2, Oct4 and Nanog expression in a dose-dependent manner (Fig. 3H and Supplementary Fig. S6A). These results implied that AurA kinase activity was related to self-renewal signaling. Further studies

should focus on identifying the mechanism by which AurA kinase activity regulates self-renewal gene expression.

In summary, the present study unveiled a potential anti-TIC function for the potential Aurora kinase inhibitor AKI603. We also presented a novel mechanism that inhibition of AurA kinase by AKI603 overcame chemoresistance through abolishing TICs in breast cancer, suggesting a novel strategy in cancer treatment.

References

1. Jemal A, Bray F, Center MM, Ferlay J, Ward E, Forman D. Global cancer statistics. *CA Cancer J Clin.* 2011;61:69-90.
2. Abdullah LN, Chow EK. Mechanisms of chemoresistance in cancer stem cells. *Clin Transl Med.* 2013;2:3.
3. Zhao Y, Butler EB, Tan M. Targeting cellular metabolism to improve cancer therapeutics. *Cell Death Dis.* 2013;4:e532.
4. Eckstein N, Servan K, Hildebrandt B, Politz A, von Jonquieres G, Wolf-Kummeth S, et al. Hyperactivation of the insulin-like growth factor receptor I signaling pathway is an essential event for cisplatin resistance of ovarian cancer cells. *Cancer Res.* 2009;69:2996-3003.
5. Williams RT, den Besten W, Sherr CJ. Cytokine-dependent imatinib resistance in mouse BCR-ABL+, Arf-null lymphoblastic leukemia. *Genes Dev.* 2007;21:2283-7.
6. Al-Hajj M, Wicha MS, Benito-Hernandez A, Morrison SJ, Clarke MF. Prospective identification of tumorigenic breast cancer cells. *Proc Natl Acad Sci U S A.* 2003;100:3983-8.
7. O'Brien CA, Pollett A, Gallinger S, Dick JE. A human colon cancer cell capable of initiating tumour growth in immunodeficient mice. *Nature.* 2007;445:106-10.
8. Boiko AD, Razorenova OV, van de Rijn M, Swetter SM, Johnson DL, Ly DP, et al. Human melanoma-initiating cells express neural crest nerve growth factor receptor CD271. *Nature.* 2010;466:133-7.
9. Dean M, Fojo T, Bates S. Tumour stem cells and drug resistance. *Nat Rev Cancer.*

2005;5:275-84.

10. Neumeister V, Rimm D. Is ALDH1 a good method for definition of breast cancer stem cells? *Breast Cancer Res Treat.* 2010;123:109-11.

11. Carmena M, Earnshaw WC. The cellular geography of aurora kinases. *Nat Rev Mol Cell Biol.* 2003;4:842-54.

12. Marumoto T, Zhang D, Saya H. Aurora-A - a guardian of poles. *Nat Rev Cancer.* 2005;5:42-50.

13. Keen N, Taylor S. Aurora-kinase inhibitors as anticancer agents. *Nat Rev Cancer.* 2004;4:927-36.

14. Katayama H, Sasai K, Kawai H, Yuan ZM, Bondaruk J, Suzuki F, et al. Phosphorylation by aurora kinase A induces Mdm2-mediated destabilization and inhibition of p53. *Nat Genet.* 2004;36:55-62.

15. Liu Q, Kaneko S, Yang L, Feldman RI, Nicosia SV, Chen J, et al. Aurora-A abrogation of p53 DNA binding and transactivation activity by phosphorylation of serine 215. *J Biol Chem.* 2004;279:52175-82.

16. Ouchi M, Fujiuchi N, Sasai K, Katayama H, Minamishima YA, Ongusaha PP, et al. BRCA1 phosphorylation by Aurora-A in the regulation of G2 to M transition. *J Biol Chem.* 2004;279:19643-8.

17. Katayama H, Wang J, Treekitkarnmongkol W, Kawai H, Sasai K, Zhang H, et al. Aurora kinase-A inactivates DNA damage-induced apoptosis and spindle assembly checkpoint response functions of p73. *Cancer Cell.* 2012;21:196-211.

18. Cammareri P, Scopelliti A, Todaro M, Eterno V, Francescangeli F, Moyer MP, et

al. Aurora-a is essential for the tumorigenic capacity and chemoresistance of colorectal cancer stem cells. *Cancer Res.* 2010;70:4655-65.

19. Millour J, de Olano N, Horimoto Y, Monteiro LJ, Langer JK, Aligue R, et al. ATM and p53 regulate FOXM1 expression via E2F in breast cancer epirubicin treatment and resistance. *Mol Cancer Ther.* 2011;10:1046-58.

20. Dontu G, Abdallah WM, Foley JM, Jackson KW, Clarke MF, Kawamura MJ, et al. In vitro propagation and transcriptional profiling of human mammary stem/progenitor cells. *Genes Dev.* 2003;17:1253-70.

21. Chou TC, Motzer RJ, Tong Y, Bosl GJ. Computerized quantitation of synergism and antagonism of taxol, topotecan, and cisplatin against human teratocarcinoma cell growth: a rational approach to clinical protocol design. *J Natl Cancer Inst.* 1994;86:1517-24.

22. Bijnsdorp IV, Giovannetti E, Peters GJ. Analysis of drug interactions. *Methods Mol Biol.* 2011;731:421-34.

23. Vickers PJ, Dickson RB, Shoemaker R, Cowan KH. A multidrug-resistant MCF-7 human breast cancer cell line which exhibits cross-resistance to antiestrogens and hormone-independent tumor growth in vivo. *Mol Endocrinol.* 1988;2:886-92.

24. Ma X, Cai Y, He D, Zou C, Zhang P, Lo CY, et al. Transient receptor potential channel TRPC5 is essential for P-glycoprotein induction in drug-resistant cancer cells. *Proc Natl Acad Sci U S A.* 2012;109:16282-7.

25. Kao J, Salari K, Bocanegra M, Choi YL, Girard L, Gandhi J, et al. Molecular profiling of breast cancer cell lines defines relevant tumor models and provides a

resource for cancer gene discovery. *PLoS One*. 2009;4:e6146.

26. Wagner RT, Xu X, Yi F, Merrill BJ, Cooney AJ. Canonical Wnt/beta-catenin regulation of liver receptor homolog-1 mediates pluripotency gene expression. *Stem Cells*. 2010;28:1794-804.

27. Anton R, Kestler HA, Kuhl M. Beta-catenin signaling contributes to stemness and regulates early differentiation in murine embryonic stem cells. *FEBS Lett*. 2007;581:5247-54.

28. Yu J, Vodyanik MA, Smuga-Otto K, Antosiewicz-Bourget J, Frane JL, Tian S, et al. Induced pluripotent stem cell lines derived from human somatic cells. *Science*. 2007;318:1917-20.

29. Takahashi K, Yamanaka S. Induction of pluripotent stem cells from mouse embryonic and adult fibroblast cultures by defined factors. *Cell*. 2006;126:663-76.

30. Fodde R, Brabletz T. Wnt/beta-catenin signaling in cancer stemness and malignant behavior. *Curr Opin Cell Biol*. 2007;19:150-8.

31. Kumar SM, Liu S, Lu H, Zhang H, Zhang PJ, Gimotty PA, et al. Acquired cancer stem cell phenotypes through Oct4-mediated dedifferentiation. *Oncogene*. 2012;31:4898-911.

32. Leis O, Eguiara A, Lopez-Arribillaga E, Alberdi MJ, Hernandez-Garcia S, Elorriaga K, et al. Sox2 expression in breast tumours and activation in breast cancer stem cells. *Oncogene*. 2012;31:1354-65.

33. Shan J, Shen J, Liu L, Xia F, Xu C, Duan G, et al. Nanog regulates self-renewal of cancer stem cells through the insulin-like growth factor pathway in human

hepatocellular carcinoma. *Hepatology*. 2012;56:1004-14.

34. Leonetti C, Biroccio A, Candiloro A, Citro G, Fornari C, Mottolese M, et al. Increase of cisplatin sensitivity by c-myc antisense oligodeoxynucleotides in a human metastatic melanoma inherently resistant to cisplatin. *Clin Cancer Res*. 1999;5:2588-95.

35. Yang L, Zhang X, Zhang M, Zhang J, Sheng Y, Sun X, et al. Increased Nanog expression promotes tumor development and Cisplatin resistance in human esophageal cancer cells. *Cell Physiol Biochem*. 2012;30:943-52.

36. Jeon HM, Sohn YW, Oh SY, Kim SH, Beck S, Kim S, et al. ID4 imparts chemoresistance and cancer stemness to glioma cells by derepressing miR-9*-mediated suppression of SOX2. *Cancer Res*. 2011;71:3410-21.

37. Crosio C, Fimia GM, Loury R, Kimura M, Okano Y, Zhou H, et al. Mitotic phosphorylation of histone H3: spatio-temporal regulation by mammalian Aurora kinases. *Mol Cell Biol*. 2002;22:874-85.

38. Meraldi P, Honda R, Nigg EA. Aurora-A overexpression reveals tetraploidization as a major route to centrosome amplification in p53^{-/-} cells. *EMBO J*. 2002;21:483-92.

39. Debnath J, Brugge JS. Modelling glandular epithelial cancers in three-dimensional cultures. *Nat Rev Cancer*. 2005;5:675-88.

40. Longley DB, Johnston PG. Molecular mechanisms of drug resistance. *J Pathol*. 2005;205:275-92.

41. Costello RT, Mallet F, Gaugler B, Sainy D, Arnoulet C, Gastaut JA, et al.

Human acute myeloid leukemia CD34⁺/CD38⁻ progenitor cells have decreased sensitivity to chemotherapy and Fas-induced apoptosis, reduced immunogenicity, and impaired dendritic cell transformation capacities. *Cancer Res.* 2000;60:4403-11.

42. Zhang L, Yang S, He YJ, Shao HY, Wang L, Chen H, et al. Fluorouracil selectively enriches stem-like leukemic cells in a leukemic cell line. *Int J Biol Sci.* 2010;6:419-27.

43. Bischoff JR, Plowman GD. The Aurora/Ipl1p kinase family: regulators of chromosome segregation and cytokinesis. *Trends Cell Biol.* 1999;9:454-9.

44. Berdnik D, Knoblich JA. Drosophila Aurora-A is required for centrosome maturation and actin-dependent asymmetric protein localization during mitosis. *Curr Biol.* 2002;12:640-7.

45. Lee CY, Andersen RO, Cabernard C, Manning L, Tran KD, Lanskey MJ, et al. Drosophila Aurora-A kinase inhibits neuroblast self-renewal by regulating aPKC/Numb cortical polarity and spindle orientation. *Genes Dev.* 2006;20:3464-74.

46. Lee DF, Su J, Ang YS, Carvajal-Vergara X, Mulero-Navarro S, Pereira CF, et al. Regulation of embryonic and induced pluripotency by aurora kinase-p53 signaling. *Cell Stem Cell.* 2012;11:179-94.

47. Cheng C, Liu ZG, Zhang H, Xie JD, Chen XG, Zhao XQ, et al. Enhancing Chemosensitivity in ABCB1- and ABCG2-Overexpressing Cells and Cancer Stem-like Cells by An Aurora Kinase Inhibitor CCT129202. *Mol Pharm.* 2012;9:1971-82.

Acknowledgements

We thank Yan Zhang, Cai-Feng Yue, Wei Zhang, Na Yang, Yuan-Min Qian, Jia-Jun Xie, Bin He, Jia-Liang Zhang, Rui Gao, Bi-Cheng Wang and other members of Liu laboratory for their critical comments and technical support.

Figure legends

Figure 1 AKI603 inhibits AurA activity, disrupts normal spindle structure and induces cell cycle arrest

(A) Chemical structure of AKI603. (B) The inhibition of AurA was tested with 3-fold dilutions of AKI603 starting from 10 μ M for a total of 10 concentrations. The kinase activity and IC₅₀s were measured with an AurA kinase assay. The mean values from three independent experiments was presented. (C) The cells were treated with various concentrations of AKI603 for 48 h. The lysates were subjected to western blotting analysis to analyze of pAurA/B (active form), AurA and AurB expression. The data were representative of three independent experiments. (D) SUM149 cells were treated with the indicated concentrations of AKI603 for 24 h. Immunofluorescence staining was performed to visualize AurA (green) and α -Tubulin (red). Nuclear DNA was stained with DAPI (blue). Morphological changes were observed by confocal fluorescence microscopy (630 \times). White arrows indicated cells with typical morphology. (E) The statistical results of (D) were presented in bar graph. The bars represented mean \pm SD of three independent experiments (N=200 in each experiment) (*: $p < 0.05$, Student's t test). (F) SUM149 cells were treated with the indicated concentration of AKI603 for 48 h. The cell cycle parameters were analyzed by flow cytometry. The upper panel showed representative flow cytometry results. The lower panel showed the statistical results. The bars represented mean \pm SD of three independent experiments (The ANOVA test, followed by the Least Significant Difference test, were used to make statistical comparisons. *: $p < 0.05$, **: $p < 0.01$, ***: $p < 0.001$).

$p < 0.001$).

Figure 2 AurA kinase activity and CD24^{Low}/CD44^{High} TICs are elevated in epirubicin-resistant MCF-7 cells.

(A) and (B) Cell sensitivity to epirubicin (48 h) was measured by an MTT assay (A) or by cell counting (B) in MCF-7 and MCF-7-Epi cells. The mean values from three independent experiments was presented. Concentrations used: 0 μ M, 0.0488 μ M, 0.0977 μ M, 0.1953 μ M, 0.3906 μ M, 0.7813 μ M, 1.5625 μ M, 3.125 μ M, 6.25 μ M, 12.5 μ M, 25 μ M and 50 μ M. (C) MCF-7 and MCF-7-Epi cells were subjected to western blotting to analyze the expression of phospho-T288 AurA (pAurA), AurA, β -catenin, c-Myc, Sox2, Oct4 and Nanog. (D) The percentage of CD24^{Low}/CD44^{High} TICs population was measured by flow cytometry in MCF-7 and MCF-7-Epi cells (upper panel). The statistical results of the flow cytometry were presented as bar graph (lower panel). The bars represented mean \pm SD of three independent experiments (***: $p < 0.001$, Student's t test).

Figure 3 AKI603 suppresses CD24^{Low}/CD44^{High} TICs and mammosphere formation.

(A) MCF-7-Epi cells were treated with the indicated concentration of AKI603 for the indicated times. The adherent cells were subjected to flow cytometric analysis to measure the CD24^{Low}/CD44^{High} TIC populations. (B) The data in (A) were presented as a line graph. The data were presented as mean \pm SD of three independent

experiments (**: $p < 0.01$, ***: $p < 0.001$, Student's *t* test). (C) Empty vector or mutant AurA plasmids (K162M or D274N) were expressed in SUM149 cells. After 72 h, the cells were harvested for western blot to detect the expression of AurA-HA and GAPDH. (D) The treatment conditions were the same as (C) and the cells were subjected to flow cytometric analysis to measure the CD24^{Low}/CD44^{High} TIC populations. The data were representative of three independent experiments (left panel). The statistical results were shown in right panel. The bars represented mean \pm SD of three independent experiments (*: $p < 0.05$, **: $p < 0.01$, The ANOVA test, followed by Least Significant Difference test, were used to make statistical comparisons.). (E) Ten-day-old MCF-7-Epi mammospheres cultured in medium containing the indicated concentration of AKI603 were photographed. Representative images were shown. (F) The diameters of the mammospheres were measured as described in the Materials and Methods. The values from three independent experiments were presented in a box plot graph and the size distribution of the mammospheres was shown. The horizontal line within each box represented the median value. The Kruskal-Wallis test, followed by Dunn's Multiple Comparison test, were used to make statistical comparisons (***: $p < 0.001$). (G) Mammospheres with diameter larger than 60 μ m were counted. The bars represented mean \pm SD of three independent experiments (***: $p < 0.001$, The ANOVA test, followed by Least Significant Difference test, were used to make statistical comparisons.). (H) MCF-7-Epi cells were treated with the indicated concentration of AKI603 for 48 h. Next, the cells were collected and subjected to western blot to analyze the expression

of pAurA, AurA, β -catenin, c-Myc, Sox2, Oct4, Nanog and GAPDH.

Figure 4 AKI603 abolishes epirubicin enriched CD24^{Low}/CD44^{High} TICs and suppresses the expression of self-renewal genes and mammosphere formation.

(A) SUM149 cells were treated with AKI603 (0.078 μ M) and/or epirubicin (0.078 μ M) for the indicated time. Adherent cells were subjected to flow cytometric analysis to measure the CD24^{Low}/CD44^{High} TIC populations. (B) The line graph showed the statistical results of the CD24^{Low}/CD44^{High} TIC population percentage measurements. The data were presented as mean \pm SD of three independent experiments. (C) The SUM149 cells were treated with the same conditions as in (A) and were subjected to western blot to analyze the expression of pAurA, AurA, β -catenin, c-Myc, Sox2, Oct4, Nanog and β -Actin. (D) Ten-day-old SUM149 mammospheres, which were cultured in medium containing AKI603 (0.078 μ M) and/or epirubicin (0.078 μ M), were photographed. Representative images were shown. (E) The box plot graph showed the mammospheres size data from three independent experiments. The horizontal line in each box represented the median value. The Kruskal-Wallis test, followed by Dunn's Multiple Comparison test, were used to make statistical comparisons (***: $p < 0.001$). (F) The mammospheres with diameter larger than 60 μ m were counted. The bar represents mean \pm SD of three independent experiments (*: $p < 0.05$, ***: $p < 0.001$, The ANOVA test, followed by Least Significant Difference test, were used to make statistical comparisons.).

Figure 5 AKI603 and epirubicin synergistically inhibit cell proliferation.

(A) and (B) The cells were treated with various concentrations of drugs alone or in combination for 6 days (single drug concentrations: 0 μ M, 0.0049 μ M, 0.0098 μ M, 0.0195 μ M, 0.0391 μ M, 0.0781 μ M, 0.1563 μ M, 0.3125 μ M, 0.625 μ M, 1.25 μ M, 2.5 μ M and 5 μ M). The growth inhibitory effects were determined by an MTT assay (A) and cell counting (B). (C) and (D) The combination indices (CI) were calculated from data obtained in (A) and (B), respectively. The plots showed the fraction of SUM149 cells that were affected by the AKI603 and epirubicin combinations. (E) SUM149 cells were treated with AKI603 (0.078 μ M) and/or epirubicin (0.078 μ M) for 6 days. The growth inhibitory effects were determined by a plate colony formation assay. Representative images were shown. (F) The statistical analysis of the plate colony formation assay was shown. The bars represented the mean \pm SD of three independent experiments (*: $p < 0.05$, **: $p < 0.01$, ***: $p < 0.001$, The ANOVA test, followed by Least Significant Difference test, were used to make statistical comparisons.). (G) and (H) SUM149 cells were maintained in three-dimensional culture condition. The cells were treated with various concentrations of drugs alone or combination for 10 days. The drug concentration settings were the same as (E). The cells were photographed, and representative images were shown in (G). The diameters of mammospheres were measured as described in the Materials and Methods and were shown in (H). The box plot graph showed the mammospheres size data from three independent experiments. The Kruskal-Wallis test, followed by Dunn's Multiple Comparison test, were used to make statistical comparisons (*: $p < 0.05$, **: $p < 0.01$, ***: $p < 0.001$).

Figure 6 AKI603 attenuates xenograft tumor growth.

(A) Nude mice bearing MCF-7-Epi xenograft tumors were treated with vehicle or AKI603 (50 mg/kg, intra-gastric administration, q.d.) from days 30 to 44 after inoculation with MCF-7-Epi cells. The estimated tumor volume was plotted versus time. (B) Tumors were removed from 5 mice in each group and were shown. (C) The weights of the dissected tumors were measured. (D) The body weights were monitored and plotted versus time. All data were presented as the mean \pm SD (n=5) (*: $p < 0.05$, **: $p < 0.01$, ***: $p < 0.001$, Student's t test).

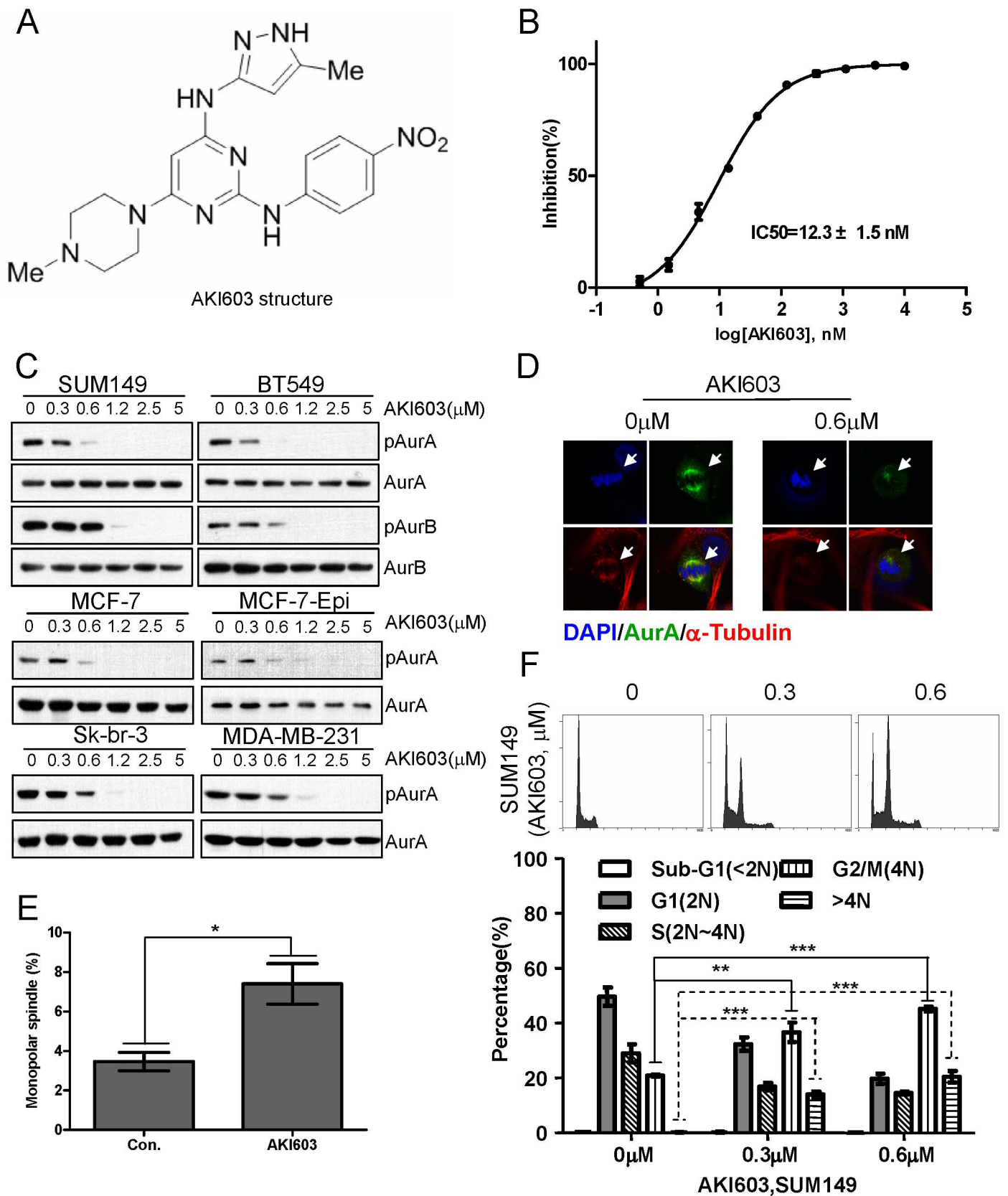


Figure 1

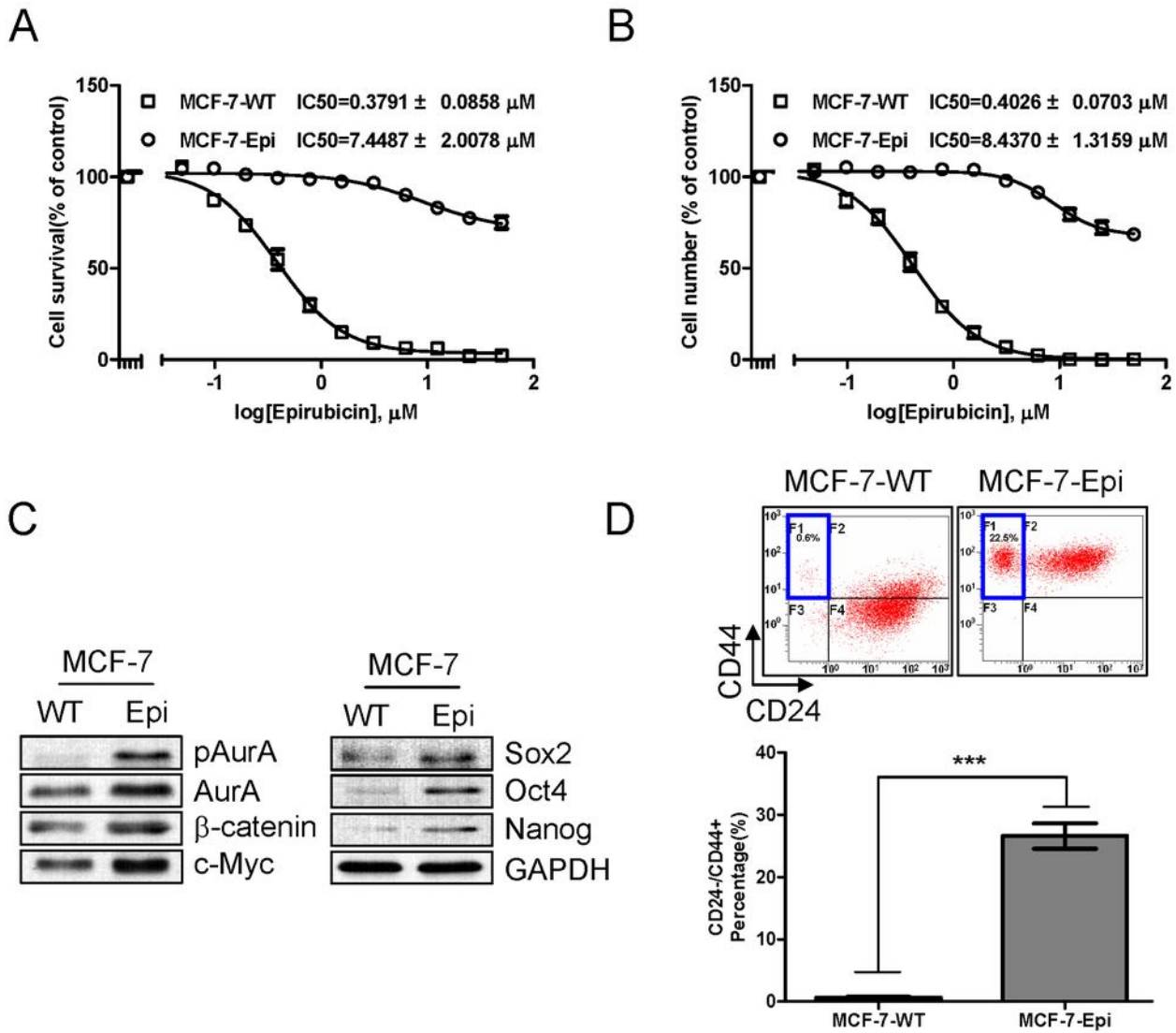


Figure 2

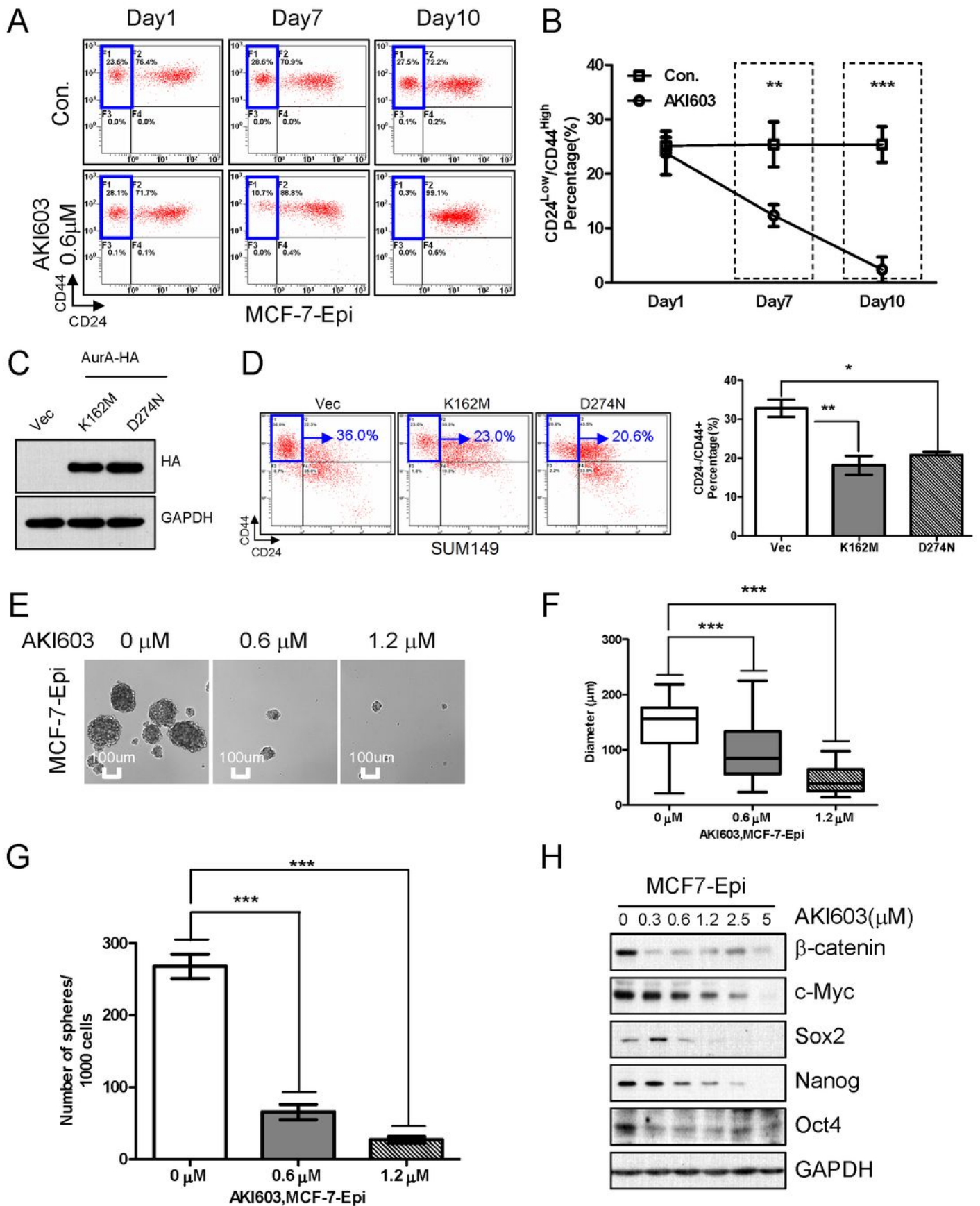


Figure 3

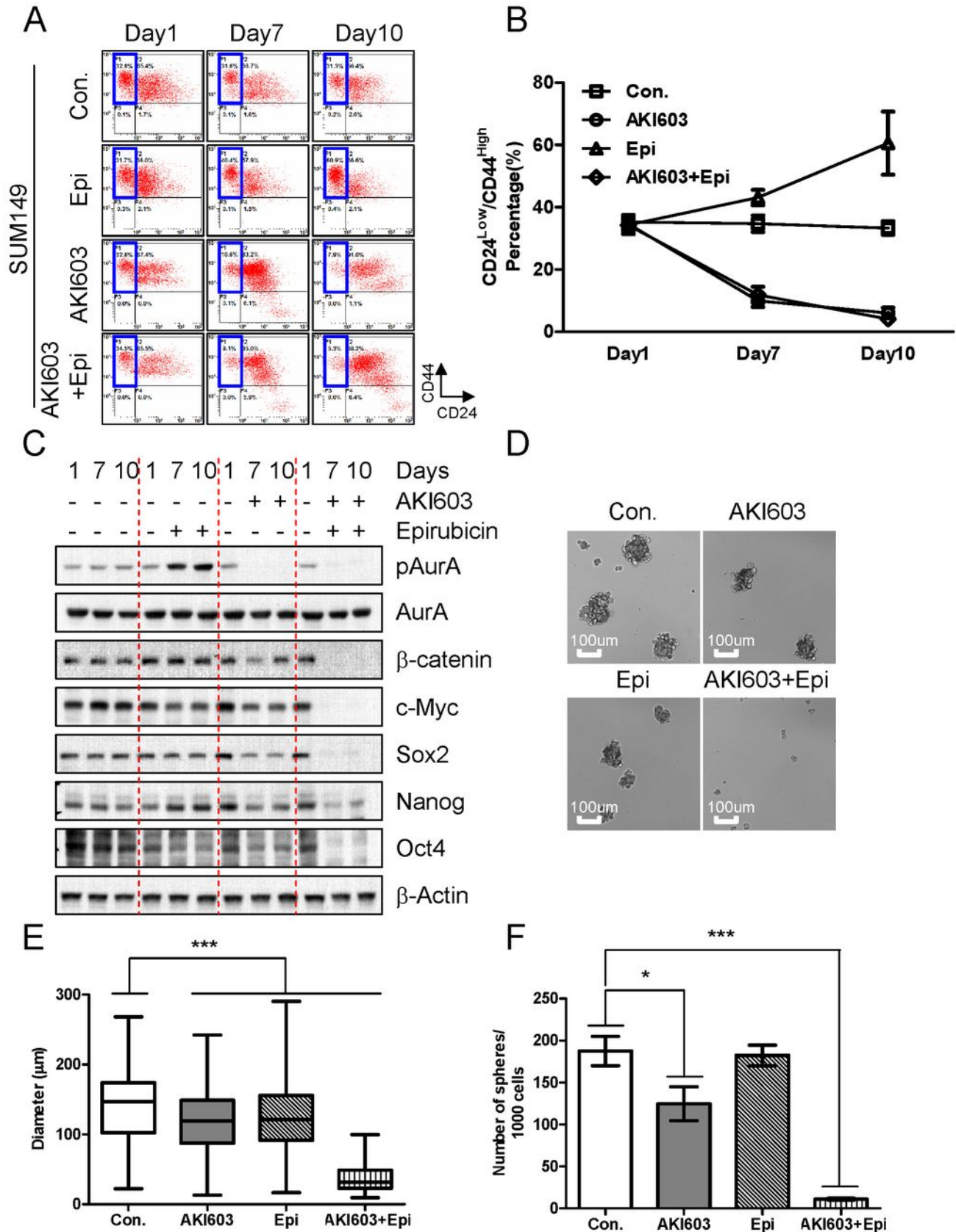


Figure 4

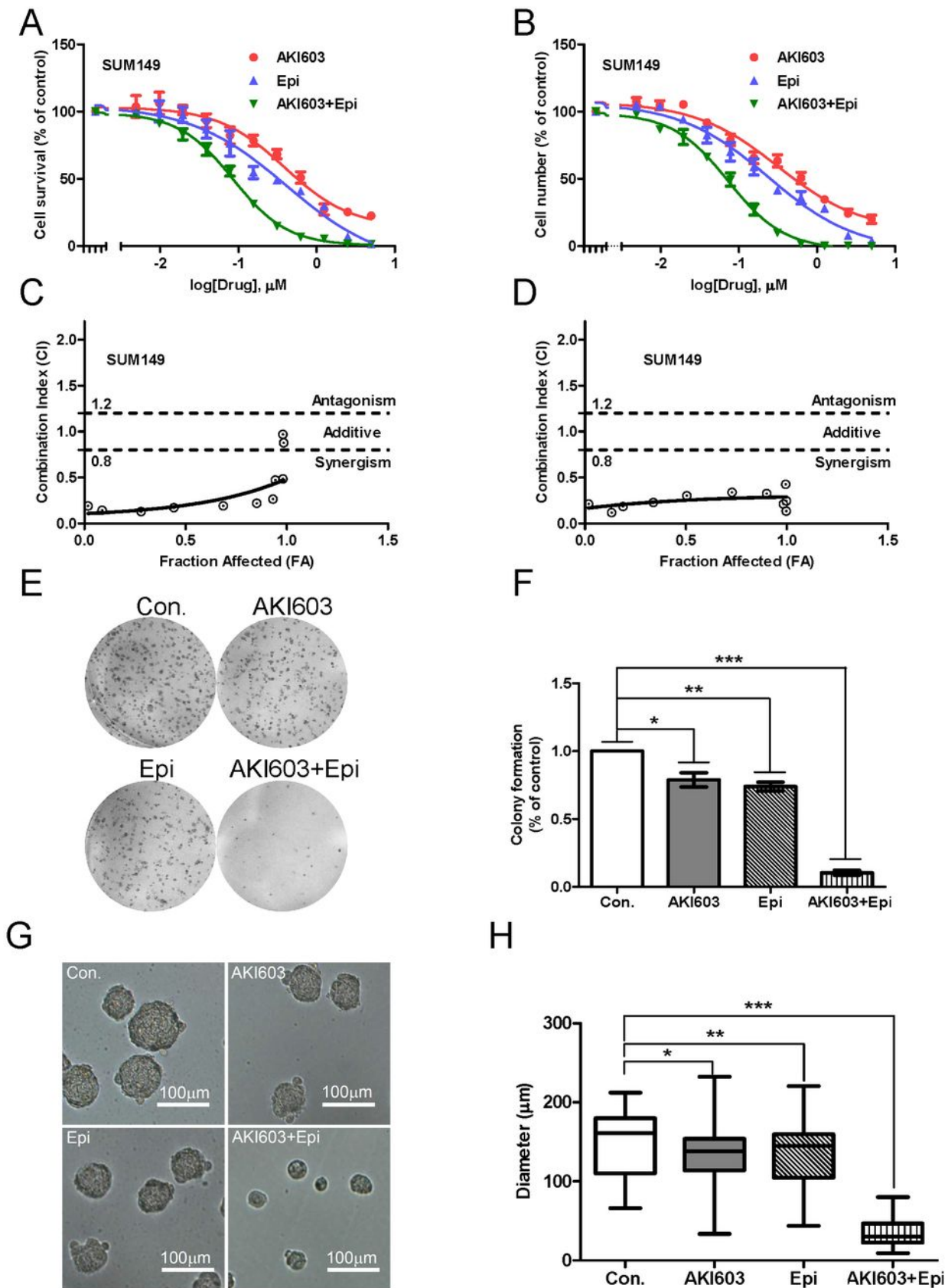


Figure 5

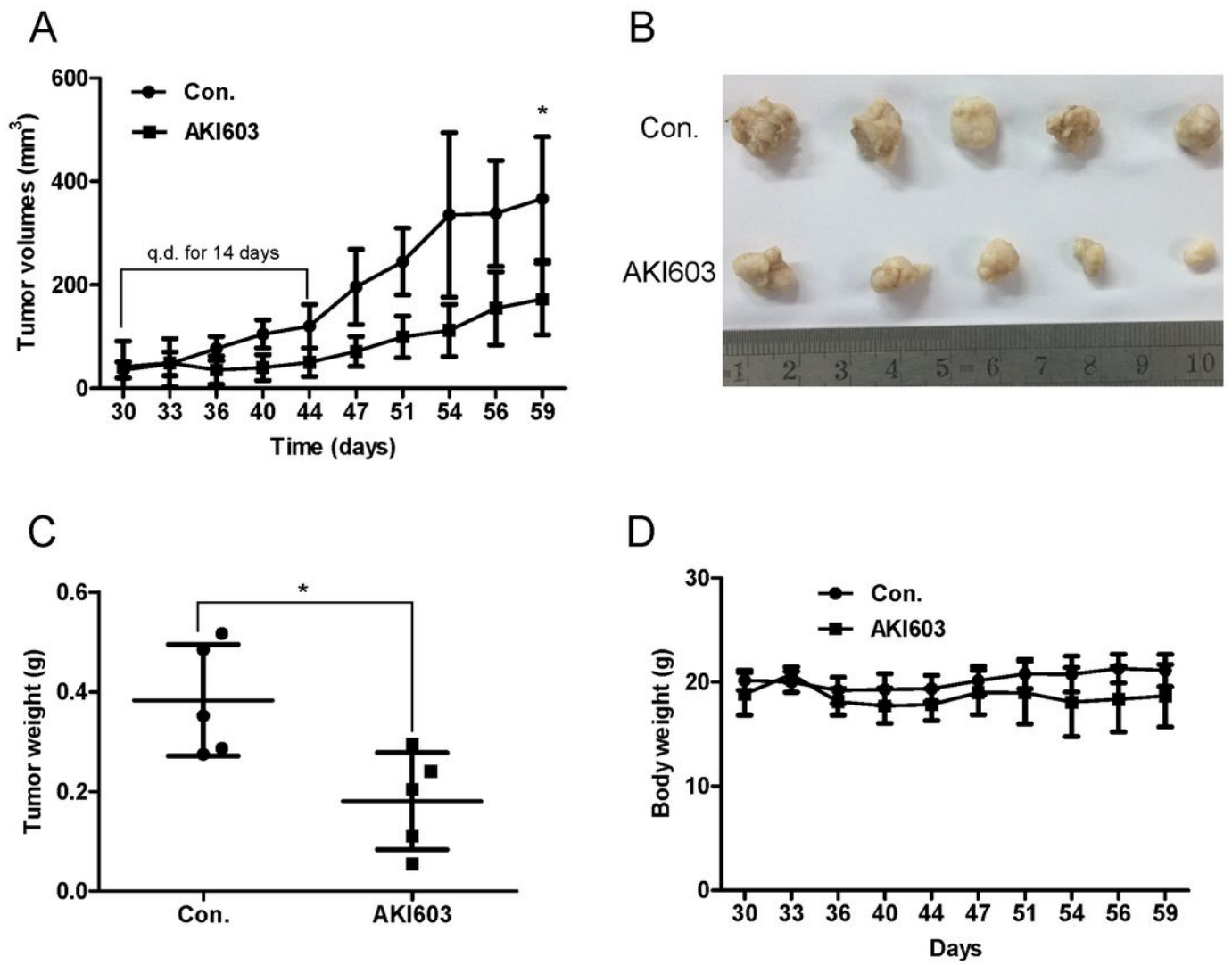


Figure 6